

000 001 002 003 004 005 A BAYESIAN NONPARAMETRIC FRAMEWORK FOR 006 LEARNING DISENTANGLED REPRESENTATIONS 007 008 009

010 **Anonymous authors**
011 Paper under double-blind review
012
013
014
015
016
017
018
019
020
021
022
023
024
025
026
027
028
029
030
031
032
033
034
035
036
037
038
039
040
041
042
043
044
045
046
047
048
049
050
051
052
053

ABSTRACT

Disentangled representation learning aims to identify and organize the underlying sources of variation in observed data. However, learning disentangled representations without any additional supervision necessitates inductive biases to solve the fundamental identifiability problem of uniquely recovering the true latent structure and parameters of the data-generating process from observational data alone. Existing methods address this by imposing heuristic inductive biases that typically lack theoretical identifiability guarantees. They also rely on strong regularization to impose these inductive biases, creating an inherent trade-off in which stronger regularization improves disentanglement but limits the latent capacity to represent underlying variations. To address both challenges, we propose a principled generative model with a Bayesian nonparametric hierarchical mixture prior that embeds inductive biases within a provably identifiable framework for unsupervised disentanglement. Specifically, the hierarchical mixture prior imposes the structural constraints necessary for identifiability guarantees, while the nonparametric formulation enables inference of sufficient latent capacity to represent the underlying variations without violating these constraints. To enable tractable inference under this nonparametric hierarchical prior, we develop a structured variational inference framework with a nested variational family that both preserves the hierarchical structure of the identifiable generative model and approximates the expressiveness of the nonparametric prior. We evaluate our proposed probabilistic model on standard disentanglement benchmarks, 3DShapes and MPI3D datasets characterized by diverse source variation distributions, to demonstrate that our method consistently outperforms strong baseline models through structural biases and a unified objective function, obviating the need for auxiliary regularization constraints or careful hyperparameter tuning.

1 INTRODUCTION

A primary objective of representation learning is not merely to perform density estimation or generate realistic samples, but to discover and characterize the latent structure inherent in observational data. This notion is formalized by disentangled representations that aim to separate the distinct, independent, and informative generative factors of variation in the data such that each latent variable is sensitive to changes in exactly one underlying factor while being relatively invariant to changes in others Bengio (2013). Disentangled representations have been shown to improve robustness and out-of-distribution generalization (Träuble et al., 2021; Li et al., 2024), sample efficiency in few-shot learning (Van Steenkiste et al., 2019; Cheng et al., 2024), domain adaptation via separation of transferable and domain-specific features (Tran & Huang, 2019; Cai et al., 2019), controllable and interpretable generation (Zhu et al., 2021; Wang et al., 2023; Zhou et al., 2025), and causal inference and fairness through explicit separation of sensitive and task-relevant factors (Cheng et al., 2024; Locatello et al., 2019a).

However, unsupervised learning of disentangled representations is fundamentally challenged with identifiability which refers to whether the true generative factors and their structure can be uniquely inferred from observed data alone. Without identifiability, different parameterizations of the generative model can produce identical distributions over observed data, making it theoretically impossible to recover the true generative factors. Prior work in nonlinear independent component analysis (Hyvärinen & Pajunen, 1999; Hyvärinen et al., 2019; Khemakhem et al., 2020), deep generative

054 modeling (Wang et al., 2021; D’Amour et al., 2022), and unsupervised disentanglement (Locatello
 055 et al., 2019b) has shown that enforcing the commonly used simple isotropic Gaussian prior in
 056 combination with a nonlinear generative function is generally insufficient to recover the true sources
 057 of variation. Without additional inductive biases, the model can learn infinitely many, potentially
 058 entangled representations that satisfy the marginal prior distribution yet fail to align with the true
 059 data-generating factors.

060 Moreover, prior works primarily impose heuristic inductive biases and typically rely on strong reg-
 061 ularization to enforce them inducing an inherent trade-off whereby stronger regularization enhances
 062 disentanglement but simultaneously restricts the representation capacity. Consequently, this mis-
 063 specification of the latent capacity either under-represents all relevant modes of variation or forces
 064 encoding of the data in a manner that conflicts with the natural structure, leading to systematic
 065 violation of the disentanglement-inducing constraints.

066 To address both these limitations we build upon the theoretical framework of Kivva et al. (2022),
 067 who prove that mixture priors provide sufficient inductive bias for identifiability in deep generative
 068 models with piece-wise affine data-generating functions. We propose a Bayesian nonparametric
 069 hierarchical mixture prior that inherits these identifiability guarantees lacking in simple Gaussian priors
 070 while simultaneously addressing the representation capacity mis-specification problem through
 071 its nonparametric formulation. To specifically learn disentangled representations, we define a fac-
 072 torized prior structure under which a nonparametric hierarchical mixture prior is placed over the
 073 space of each generative factor independently, such that mixture components correspond to discrete
 074 variations of the respective factor. Consistent with the principles of classical factor analysis, this
 075 factorized structure entails that observations are generated through the combinatorial composition
 076 of factor-specific mixture components, with each observation determined by a unique combination
 077 of components across all generative factors Hsu et al. (2024a). Critically, the factorized prior struc-
 078 ture facilitates the orthogonal encoding of factor-specific variations. The nonparametric formulation
 079 allows the complexity of factor-specific mixtures to remain unspecified *a priori*—a characteristic
 080 analogous to species discovery in unexplored ecosystems, where the number and types of species
 081 present cannot be predicted in advance. This formulation endows our model with universal approx-
 082 imation capabilities, ensuring that the identifiable architecture is, in principle, expressive enough to
 083 recover the natural underlying structure of the data.

084 For tractable inference under this nonparametric hierarchical prior, we develop a structured vari-
 085 ational inference framework with a nested variational family. The structured inference framework
 086 preserves the hierarchical structure of the identifiable generative model thereby enabling joint op-
 087 timization of the prior and deep generative model parameters within a unified objective function.
 088 The nested formulation enables the variational distribution to approximate the expressiveness of the
 089 nonparametric prior while maintaining computational tractability.

090 Empirically, we show that this hierarchical mixture prior provides substantially stronger inductive
 091 biases enabling the learning of modular and compact disentangled representations that enhance in-
 092 terpretability. Our results on two image datasets with distinct factor distributions further demon-
 093 strate that the nonparametric hierarchical mixture prior and the corresponding inference framework
 094 provide sufficient inductive bias without additional computationally expensive auxiliary inductive
 095 biases or careful manual tuning of regularization hyperparameters

096 2 NONPARAMETRIC BAYESIAN QUANTIZATION FOR AUTOENCODERS

097 Prior work (Hsu et al., 2024a;b) introduce inductive biases that encourage disentangled representa-
 098 tion learning by structuring the latent space as a factorized Cartesian product of discrete sets, where
 099 each latent dimension is independently quantized through separate learnable codebooks. This latent
 100 quantization architecture restricts the encoder to constructing representations through combinato-
 101 rial selection from small finite codebooks of scalar embeddings. This, consequently, constrains the
 102 decoder to assign consistent semantic meanings to the embeddings, such that each codebook en-
 103 codes a single factor of variation with the embeddings representing specific variations within the
 104 factor. For this architectural design to serve as an effective inductive bias for learning disentangled
 105 representations, the size of each codebook C_i , and thus the support of the corresponding discrete
 106 latent variable z_i , used to index the codebook embeddings, is fixed and kept small. While this de-
 107 sign choice encourages parsimonious representations, factors with variations larger than the size of

108 a single codebook must necessarily be distributed across multiple codebooks, reducing the interpretability
 109 of the learned factors.
 110

111 To address this limitation and ensure that each generative factor, with potentially unbounded number
 112 of variations, can be encoded in a single codebook, we propose a principled probabilistic formula-
 113 tion in which each codebook possesses theoretically infinite number of embeddings. Specifically,
 114 we place a nonparametric Dirichlet Process (DP) (Ferguson, 1973; Sethuraman, 1994) over each dis-
 115 crete codebook and use the stick-breaking construction to define a valid probability mass function
 116 with countably infinite support for the discrete latent variables z . To enable principled uncertainty
 117 quantification within this nonparametric framework, each scalar embedding is instead a stochastic
 118 variable governed by a probability distribution rather than a fixed point estimate. To realize this, we
 119 use the base distribution of the DP to generate the countably infinite set of parameters that define
 120 the distributions from which these stochastic embeddings are sampled. This formulation naturally
 121 induces a Dirichlet Process Mixture Model (DPMM) prior (A.1.1) over the embedding space, where
 122 each codebook’s embeddings are modeled as samples drawn from an infinite-component mixture
 123 distribution.

124 To preserve the inductive biases, that makes latent quantization effective, within our nonparamet-
 125 ric framework, we propose nested variational family-based inference for posterior approximation.
 126 During inference with this nested family, each codebook is initialized with a single component or
 127 embedding parameter. When the model encounters data requiring greater representational capacity,
 128 new components are greedily added to the codebook. This greedy expansion allows the model to
 129 gradually adapt its capacity to the complexity of the generative factor represented by the codebook,
 thereby providing a stronger inductive bias.
 130

131 In the following sections, we first formalize the hierarchical Bayesian nonparametric prior govern-
 132 ing the embedding space and derive the corresponding generative model. We next formalize the
 133 structured variational family, specifically designed to accurately approximate the posterior distribu-
 134 tion with hierarchical structured priors. Finally, we present the nested extension of this structured
 135 variational family which enables principled incremental expansion of the representational capacity
 while preserving inductive biases of latent quantization.
 136

2.1 NONPARAMETRIC PRIOR

138 We adopt the inductive bias of latent quantization (For a prior on vector-quantized and latent-
 139 quantized autoencoder please refer to Section A.1.2) by decomposing each datapoint’s d -
 140 dimensional encoder output vector into component scalars, where each scalar is independently
 141 quantized using a separate codebook C_i . The discrete latent variable z is defined as an element
 142 of the Cartesian product of component discrete sets $\mathbf{z} \in Z_1 \times \dots \times Z_d$ where each discrete variable
 143 $z_i \in Z_i = \{1, \dots, |C_i|\}$, $\forall i \in \{1, \dots, d\}$ indexes the embeddings of codebook C_i . Formally, we
 144 define a nonparametric prior over the parameter space Θ of the mixture components for each code-
 145 book C_i using the Dirichlet Process $DP(\alpha, G_0)$. For each codebook C_i , we use the stick-breaking
 146 construction to generate an infinite sequence of stick-breaking proportions $\beta_i = \{\beta_{i,k}\}_{k=1}^{\infty}$, with
 147 each $\beta_{i,k}$ independently drawn from a Beta distribution with concentration parameter α control-
 148 ling the expected number of active mixture components. Concurrently, the embeddings parameters
 149 $\theta_i = \{\theta_{i,k}\}_{k=1}^{\infty}$ are independently sampled from a continuous base distribution $G_0(\lambda)$, defined over
 the parameter space Θ :
 150

$$\beta_{i,k} \mid \alpha \sim p(\beta \mid \alpha) = \text{Beta}(1, \alpha), \quad \theta_{i,k} \mid \lambda \sim p(\theta \mid \lambda) = G_0(\lambda), \quad \forall i \in \{1, \dots, d\}, \forall k \in \mathbb{N}$$

151 The stick-breaking proportions β_i are then used to define the countably infinite set of mixture
 152 weights that specify a valid probability mass function over the discrete latent variables z_i , replacing
 153 the fixed uniform prior of VQVAE and its variants. Conditional on the discrete variable $z_i = k$, the
 154 corresponding embedding e_i is sampled from the k -th mixture component distribution $p(e \mid \theta_{i,k})$.
 155 This generative process for the discrete latent variable z_i and the corresponding embedding e_i asso-
 156 ciated with codebook C_i is formalized as follows:
 157

$$z_i = k \mid \beta_i \sim p(z_i = k \mid \beta_i) = \beta_{i,k} \prod_{j=1}^{k-1} (1 - \beta_{i,j}), \quad e_i \sim p(e \mid z_i, \theta_i) = \prod_{k=1}^{\infty} (p(e \mid \theta_{i,k}))^{\mathbf{1}_{[z_i=k]}}$$

161 We choose the Gaussian distribution with unknown mean and precision parameters $\theta_k = \{\mu_k, s_k\}$,
 where μ_k denotes the mean and s_k the precision (inverse variance), to sample the embedding vec-

162 tors. Following conjugacy structure, we choose the base distribution G_0 for sampling these
 163 parameters θ to be a Normal–Gamma distribution $G_0(\lambda) = \mathcal{N}\mathcal{G}(m_0, \kappa_0, \nu_0, w_0)$ which serves as a
 164 conjugate prior to the Gaussian likelihood with unknown mean and precision. Importantly, the Nor-
 165 mal–Gamma prior simultaneously captures uncertainty over both the mean and precision par-
 166 ameters, facilitating efficient joint sampling, and simplifies Bayesian inference by enabling closed-form
 167 posterior updates. We define the data-generating distribution as $p_{\theta_g}(x | e) \sim \mathcal{N}(g_{\theta_g}(e), \sigma^2 \mathbf{I})$ where
 168 $g_{\theta_g} : \mathcal{E} \rightarrow \mathcal{X}$ is a nonlinear mapping parameterized by θ_g that transforms the embedding vectors
 169 $e \in \mathcal{E}$ into the observation space \mathcal{X} . The joint distribution over the observed data x , latent em-
 170 beddings e , discrete latent variables z , stick-breaking proportions β and embedding distribution
 171 parameters θ factorizes according to the hierarchical generative model as follows:

$$172 \quad p(x, e, z, \beta, \theta | \alpha, \lambda) = p_{\theta_g}(x | e) \prod_{i=1}^d p(e_i | z_i, \theta_i) p(z_i | \beta_i) \prod_{k=1}^{\infty} p(\beta_{i,k} | \alpha) p(\theta_{i,k} | \lambda) \quad (1)$$

175 This hierarchical structure induces a natural partitioning of the embedding space into clusters cor-
 176 responding to the mixture components and provides a principled probabilistic framework to model
 177 the underlying discrete latent structure.

179 2.2 VARIATIONAL INFERENCE

181 To enable a computationally efficient posterior approximation for nonparametric priors (for a prior
 182 on variational inference for DPMMS please refer to the Preliminary section A.1), Blei & Jordan
 183 (2006); Hoffman et al. (2013) approximate the infinite-dimensional stick-breaking process using a
 184 truncated stick-breaking variational family. This formulation introduces an explicit truncation level
 185 T by fixing the stick-breaking proportion at position T to one $q_{\nu_\beta}(\beta_T = 1) = 1$, which implicitly
 186 forces all subsequent stick lengths $\{\beta_k\}_{k>T}$ and the corresponding mixture weights to zero, thus
 187 limiting the mixture components to T . Further, this approach renders inference tractable with the use
 188 of fully factorized variational distributions; which impose strong independence constraints among
 189 latent variables, including those with hierarchical dependencies. The approach of Hoffman & Blei
 190 (2015) relaxes this mean-field assumption to allow dependencies between hierarchical latent vari-
 191 ables, yielding more accurate posterior approximations and reducing bias; while lowering sensitivity
 192 to initialization and hyperparameters. We adapt this structured variational inference framework to
 193 preserve the hierarchical dependencies in our formulation, specifically between the stick-breaking
 194 proportions β and the discrete latent variables z as well as between the discrete variable z , the
 195 components parameters θ and the embeddings e as detailed below:

$$196 \quad q_{\nu}(e, z, \beta, \theta) = q(e | z, \theta) q(z | \beta) \prod_{k=1}^{T-1} q_{\nu_{\beta,k}}(\beta_k) \prod_{k=1}^T q_{\nu_{\theta,k}}(\theta_k) \quad (2)$$

199 Truncated variational families make inference in infinite-mixture models tractable by restricting the
 200 variational distribution to a fixed number T of mixture components. The intuition that increasing
 201 the truncation level monotonically increases the ELBO, with more mixture components allowing
 202 q to better approximate the true nonparametric posterior, motivates practitioners to choose high
 203 truncation levels. However, this intuition fails when an optimal truncation level exists, particularly
 204 for data generated by a finite mixture. Moreover, the truncated variational families are not nested;
 205 the variational family with truncation level T is not a subset of the family with truncation level $T+1$.
 206 Therefore, increasing T beyond the optimal level does not necessarily yield a better approximation
 207 and undermines the inductive bias of quantizing with a small set of latent embeddings, critical for
 208 learning disentangled representations.

208 Therefore, we employ the nested variational family framework of Kurihara et al. (2006), which de-
 209 fines an infinite-dimensional variational parameter space $\{\nu_{\beta,k}, \nu_{\theta,k}\}_{k=1}^{\infty}$, to support an unbounded
 210 number of mixture components using parameter tying.

$$212 \quad q_{\nu}(\beta) = \prod_{k=1}^T q_{\nu_{\beta,k}}(\beta_k) \prod_{k=T}^{\infty} p(\beta_k | \alpha), \quad q_{\nu}(\theta) = \prod_{k=1}^T q_{\nu_{\theta,k}}(\theta_k) \prod_{k=T}^{\infty} p(\theta_k | \lambda) \quad (3)$$

215 When data are associated only with the first T components, the variational parameters for all com-
 216 ponents $k > T$ are tied to their corresponding prior values, such that $q_{\nu_{\beta,k}}(\beta_k) = p(\beta | \alpha)$ and

$q_{\nu_{\theta,k}}(\theta_k) = p(\theta | \lambda)$. This parameter tying effectively constrains the variational distributions beyond the implicit truncation level T to the prior distribution. This constraint ensures that although the variational distribution theoretically includes an unbounded number of mixture components, we only need to represent and optimize parameters up to the implicit truncation level T . Crucially, data belonging to components beyond the truncation level T , can be assigned to the infinite components, with their parameters tied to the prior. This enables our inference algorithm to proceed greedily, starting with $T = 1$ and incrementally adding components only when they yield a significant improvement in the empirical ELBO. This process of incrementally adding components is continued until all data is assigned to components within truncation level T and no data is assigned to the prior. Notably, under this nested formulation, codebook components that fail to encode meaningful variations collapse back to their prior distribution during training.

For a single data point, the ELBO, estimated using Monte Carlo samples, under this hierarchical, structured, nested variational family q_ν , given the generative model in Equation equation 1, can be expressed as:

$$\mathcal{L} = \frac{1}{N} \mathbb{E}_{q_{\nu_\beta}} \left[\log \frac{p(\beta | \alpha)}{q_{\nu_\beta}(\beta)} \right] + \frac{1}{N} \mathbb{E}_{q_{\nu_\theta}} \left[\log \frac{p(\theta | \lambda)}{q_{\nu_\theta}(\theta)} \right] + \mathbb{E}_{q_\nu} \left[\log \frac{p_{\theta_g}(x | e) p(e | z, \theta) p(z | \beta)}{q(e | z, \theta) q(z | \beta)} \right]$$

2.3 THE ALGORITHM

Efficient inference algorithms for hierarchical models rely on the use of conjugate exponential family data likelihoods, which preserve tractable structure. Specifically, hierarchical models where the latent variables follow distributions from the exponential family and the generative model is conjugate to the prior, the resulting conditional posterior distributions remain within the same exponential family as the prior, thereby facilitating such efficient inference. However, for general neural network observation likelihoods, such as p_{θ_g} , the absence of such conjugacy structure significantly increases the computational complexity of inferring the latent variables requiring multiple passes through the generative model. To ensure computational tractability while using general non-conjugate observation likelihoods with structured latent variable priors, we use deep amortized recognition networks $h(x; \phi)$ of Johnson et al. (2016). For each datapoint, these networks output local conjugate likelihood potentials \hat{p}_ϕ , as defined in Equation 4 unlike standard variational autoencoder encoders that directly output variational distribution parameters. These conjugate potentials replace the original non-conjugate observation likelihoods during inference, and are combined with the structured latent variable prior using efficient message-passing algorithms, thereby preserving the tractability of conjugate graphical model inference.

$$\hat{p}_\phi(e | x) = \prod_{i=1}^d \hat{p}_\phi(e_i | x) = \prod_{i=1}^d \exp\{\langle h_i(x; \phi), t_e(e_i) \rangle\} \quad (4)$$

This independence structure of the recognition network, enables the inference of local latent variables $\{e_i, z_i\}$ associated with each codebook C_i independently of the other codebooks. With this structural constraint, the data-likelihood third term of the ELBO (2.2) with local latent variables decomposes into a sum over individual dimensions:

$$\mathcal{L}_i = \mathbb{E}_{q_{\nu_\beta}(\beta)q(z_i | \beta)} \left[\log \frac{p(z_i | \beta)}{q(z_i | \beta)} + \mathbb{E}_{q_{\nu_\theta}(\theta)q(e_i | z_i, \theta)} \left[\log \frac{p(e_i | z_i, \theta)}{q(e_i | z_i, \theta)} + \log \hat{p}_\phi(e_i | x) \right] \right] \quad (5)$$

Similar to the work of Hoffman & Blei (2015), we observe that, with the global latent variables β and θ and the local latent variable z_i held fixed, the second term—dependent on the latent variable e_i —can be expressed as a variational lower bound on the conditional marginal likelihood associated with the conjugate potential of that dimension.

$$\begin{aligned} & \mathbb{E}_{q(e_i | z_i, \theta)} \left[\log \frac{p(e_i | z_i, \theta)}{q(e_i | z_i, \theta)} + \hat{p}_\phi(e_i | x) \right] \\ &= -D_{\text{KL}}(q(e_i | z_i, \theta) \| \hat{p}_\phi(e_i | x, z_i, \theta)) + \log \hat{p}_\phi(x_i | z_i, \theta) \leq \log \hat{p}_\phi(x_i | z_i, \theta) \end{aligned} \quad (6)$$

with the local posterior distribution of e_i conditioned on the data and the latent variables, defined as

$$\hat{p}_\phi(e_i | x_i, z_i, \theta) = \frac{\hat{p}_\phi(e_i | x_i) p(e_i | z_i, \theta)}{\hat{p}_\phi(x_i | z_i, \theta)} \quad (7)$$

270 Here, the marginal likelihood of the conjugate potential defined as $\hat{p}_\phi(x_i | z_i, \theta) = \int \hat{p}_\phi(e_i | x_i, z_i, \theta) p(e_i | z_i, \theta) de_i$ to ensure that the posterior $\hat{p}_\phi(e_i | x_i, z_i, \theta)$ is a valid probability distribution. 271 Since the Kullback-Leibler (KL) divergence is non-negative, choosing the variational distribution 272 $q(e_i | z_i, \theta)$ to be exactly equal to the local posterior $\hat{p}_\phi(e_i | x_i, z_i, \theta)$ minimizes the KL divergence 273 to zero and yields the tightest possible lower bound on the local ELBO. 274

$$275 \begin{aligned} q(e_i | z_i, \theta) &= \hat{p}_\phi(e_i | x_i, z_i, \theta) \\ 276 &= \exp \{ \langle \eta_e(z_i, \eta_\theta(\theta), \phi), t_e(e) \rangle - A_e(\eta_e(z_i, \eta_\theta(\theta), \phi)) \} \end{aligned} \quad (8)$$

278 where the natural parameters $\eta_e(z_i, \eta_\theta(\theta), \phi)$, defined as 279

$$280 \eta_e(z_i, \eta_\theta(\theta), \phi) = \sum_{k=1}^T \mathbf{1}_{[z_i=k]} \eta_\theta(\theta_k) + h_i(x_i; \phi) \\ 281 \\ 282$$

283 This formulation explicitly expresses the variational distribution $q(e_i | z_i, \theta)$ as an exponential 284 family distribution resulting from combining the conjugate observation likelihood with the 285 structured latent prior distribution. It is worth noting that for effective partitioning of the data through 286 quantization, instead of propagating embeddings to the decoder which are sampled from the 287 variational distribution $q(e_i | z_i, \theta)$, we propagate embeddings sampled from their prior distribution 288 $p(e_i | z_i, \theta)$. This forces the representations to cluster around the prior and encoding variations 289 common to all data belonging to the same cluster. 290

291 It is worth noting that for effective data partitioning through representation quantization, we propagate 292 embeddings sampled from the prior distribution $p(e_i | z_i, \theta)$ to the decoder, rather than from the 293 variational distribution $q(e_i | z_i, \theta)$. This approach forces the representations to encode variations 294 common to all data belonging to the same cluster, rather than datapoint-specific information. With 295 this choice of variational distribution for e_i , it is crucial to note that the local ELBO can be further 296 expressed as a variational lower bound on the marginal likelihood of the data, conditioned on the 297 global variable β with respect to the latent variable z_i . 298

$$299 \begin{aligned} \mathcal{L}_i &= \mathbb{E}_{q_{\nu_\beta}(\beta)q(z_i|\beta)} \left[\log \frac{p(z_i | \beta)}{q(z_i | \beta)} + \mathbb{E}_{q_{\nu_\theta}(\theta)} [\log \hat{p}_\phi(x_i | z_i, \theta)] \right] \\ 300 &= -D_{\text{KL}}(q(z_i | \beta) \| \hat{p}_\phi(z_i | x_i, \beta)) + \log \hat{p}_\phi(x_i | \beta) \leq \log \hat{p}_\phi(x_i | \beta) \end{aligned} \quad (9)$$

302 Therefore, similar to the variational distribution of e_i , the variational distribution of z_i can be set to 303 the local optimal value given by 304

$$305 \begin{aligned} \log q(z_i = k) &\propto E_{q_{\nu_\theta}(\theta)} \log \hat{p}_\phi(x_i | z_i = k, \theta) \\ 306 &= A_e(\eta_\theta(\theta_k) + h_i(x_i; \phi)) - A_e(\eta_\theta(\theta_k)) \end{aligned} \quad (10)$$

307 The use of structured variational inference with deep amortized recognition networks enables the 308 variational distributions over local latent variables to be set to their locally optimal values, thereby 309 ensuring tractable and efficient inference. At each iteration, we first sample the global parameters 310 β and θ from their variational distributions $q_{\nu}(\beta)$ and $q_{\nu}(\theta)$ respectively and use the samples to 311 compute the local variational distributions. 312

313 However, in the context of structured variational inference, as noted by Hoffman & Blei (2015) exact 314 inference over the global variables is generally intractable due to the restored dependencies between 315 global and local variables. Moreover, the use of recognition networks in place of the non-conjugate 316 likelihood generative functions necessitates gradient-based estimation of global parameters. As a 317 result, we use low-variance Monte Carlo estimators to approximate the required expectations and 318 efficiently implement this using the reparameterization trick, which enables gradient-based optimiza- 319 tion of the variational parameters. For approximate posterior inference of the global variables, 320 we use stochastic gradient-based optimization methods equipped with adaptive preconditioning 321 matrices, such as RMSProp (Graves, 2013) and Adam Adam et al. (2014). These optimizers facilitate 322 efficient updates by scaling the gradients according to the geometry of the parameter space. To 323 further enhance convergence and stability, we select the step-size following the recommendations 324 of Mandt et al. (2017), which provide principled guidance for optimal learning rates for posterior 325 inference. 326

324 **3 EXPERIMENTS**

325

326 In this section, we present experiments designed to empirically assess whether the hierarchical
 327 Bayesian nonparametric approach to latent quantization provides effective inductive biases for
 328 learning interpretable disentangled representations. Specifically, we evaluate whether our approach
 329 achieves comparable performance relative to prior work which impose equivalent inductive biases
 330 through multiple, distinct regularization terms.

331 **Datasets.** Our experimental framework systematically addresses these questions through comprehensive
 332 quantitative evaluations conducted on two benchmark datasets labeled with ground-truth
 333 source information. Each dataset is constructed from mutually independent sources through a deterministic
 334 data generation process. In particular, we use the 3DShapes (Burgess & Kim, 2018) dataset
 335 of 3D shapes generated from six ground-truth independent latent factors with approximately uniform
 336 and small number of variations. Additionally, we use the MPI3D dataset (Gondal et al., 2019),
 337 collected from a real-world robotic environment, which exhibits a power-law distribution across the
 338 number of variations of different factors. Specifically, a few factors contain extensive variations
 339 (e.g., 40 discrete values for each rotational degrees of freedom), while the majority possess substantially
 340 fewer variations (e.g., 2-6 values for object properties).

341 **Prior Methods.** We evaluate our proposed approach against several state-of-the-art methods that
 342 incorporate distinct inductive biases for unsupervised disentanglement. Specifically, we compare
 343 to β -VAE Higgins et al. (2017) and β -TCVAE Chen et al. (2018) which enforces disentanglement
 344 through information-theoretic regularization encouraging independence across latent dimensions.
 345 We further consider BioAE Whittington et al. (2022), which introduces biologically inspired
 346 constraints—namely nonnegativity and energy efficiency—to promote compact representations enforcing
 347 neurons to become selective for single factors of task variation, together with a grid-like structural
 348 constraint as an architectural inductive bias. In addition, we examine QLAE Hsu et al. (2024a),
 349 which introduces an architectural bias based on latent quantization, and subsequently Tripod Hsu
 350 et al. (2024a), which combines latent quantization with additional inductive biases enforcing independence
 351 among latent variables as well as constraining the functional mapping from latent representations to the data space. For a concise prior on the disentanglement metrics and the different
 352 properties measured please refer to Section A.3.

353 **Quantitative Comparison with Prior Methods.** The experimental evaluation demonstrates that
 354 the proposed Bayes-QLAE consistently outperforms most baseline methods across both datasets
 355 in terms of modularity metrics (InfoM and D), with the notable exception of achieving competitive
 356 performance relative to QLAE and Tripod (Table 1 and Table 2). The observed improvements
 357 in compactness (InfoC) are particularly pronounced when compared to the baseline QLAE, demon-
 358 strating the effectiveness of the nonparametric prior in adapting to the complexity of underlying gener-
 359 ative factors while maintaining consistency in modularity. Contrary to the position advanced by
 360 the authors of QLAE, who prioritize modularity/disentanglement over compactness/completeness
 361 through specific architectural design choices, we argue that achieving interpretable representations
 362 that faithfully capture mutually independent generative factors requires balanced weighting of both
 363 modularity and compactness metrics. With competitive explicitness and informativeness measures,
 364 Bayes-QLAE demonstrates performance consistent with QLAE and Tripod while substantially out-
 365 performing alternative approaches, reinforcing the efficacy of latent quantization for disentangled
 366 representation learning.

367 It is worth noting that Tripod achieves its superior modularity and compactness performance through
 368 the application of a Normalized Hessian Penalty, which necessitates multiple forward passes through
 369 the generative network, thereby incurring additional computational overhead. In contrast, Bayes-
 370 QLAE achieves competitive performance through architectural inductive biases alone, without re-
 371quiring additional regularization terms. Furthermore, Tripod’s disentanglement performance, partic-
 372 ularly in modularity and compactness dimensions, exhibits sensitivity to quantization level hyper-
 373 parameters, which must be specified a priori. Conversely, Bayes-QLAE demonstrates adaptive
 374 behavior that automatically learns quantization levels from the data while maintaining robustness
 375 across evaluation metrics.

376 We observe that the performance improvement of Bayes-QLAE is notably more pronounced on
 377 the 3DShapes dataset compared to the MPI3D dataset, where factor variations are characterized
 378 by a power-law distribution. This differential performance suggests that the underlying distribu-

tional properties of the generative factors significantly influence the efficacy of the nonparametric prior. We hypothesize that replacing the Dirichlet Process prior with a more flexible, generalized prior such as the Pitman–Yor process—which allows for a richer clustering structure and can model power-law behaviors—may yield further performance gains. We perform detailed ablation studies to systematically isolate and quantify the inductive biases contributed by each component of our hierarchical Bayesian nonparametric framework in Section A.2. ¹

model	InfoM	InfoC	InfoE	D	C	I
β -VAE	0.62 \pm .02	0.44 \pm .03	0.93 \pm .02	0.58 \pm .02	0.42 \pm .02	0.97 \pm .02
β -TCVAE	0.65 \pm .03	0.56 \pm .02	0.91 \pm .02	0.56 \pm .02	0.46 \pm .02	0.95 \pm .02
BioAE	0.58 \pm .02	0.42 \pm .02	0.90 \pm .01	0.48 \pm .01	0.39 \pm .02	0.91 \pm .02
QLAE	0.84 \pm .02	0.49 \pm .01	0.97 \pm .01	0.79 \pm .01	0.56 \pm .01	0.97 \pm .01
Tripod	0.91 \pm .03	0.58 \pm .03	0.96 \pm .02	0.80 \pm .03	0.63 \pm .03	0.97 \pm .02
Bayes-QLAE	0.91 \pm .03	0.61 \pm .02	0.95 \pm .02	0.84 \pm .03	0.65 \pm .03	0.97 \pm .02

Table 1: Disentanglement metrics measured in InfoMEC and DCI for 3Dshapes dataset. For each metric a higher score is better. The scores for all the models were averaged across 5 runs with different random seeds with intervals denoting 95% confidence intervals of the mean estimated assuming a t-distribution. The results for the VQE-based and QLAE-based models are obtained using the hyperparameter settings and experimental conditions as described in Locatello et al. (2019b) and Hsu et al. (2024a;b) respectively.

model	InfoM	InfoC	InfoE	D	C	I
β -VAE	0.41 \pm .03	0.40 \pm .03	0.68 \pm .03	0.24 \pm .03	0.19 \pm .03	0.80 \pm .03
β -TCVAE	0.48 \pm .03	0.46 \pm .03	0.62 \pm .03	0.27 \pm .03	0.24 \pm .03	0.79 \pm .03
BioAE	0.44 \pm .03	0.38 \pm .02	0.61 \pm .03	0.26 \pm .02	0.14 \pm .02	0.77 \pm .02
QLAE	0.52 \pm .02	0.43 \pm .02	0.68 \pm .04	0.38 \pm .04	0.34 \pm .04	0.81 \pm .04
Tripod	0.59 \pm .05	0.54 \pm .05	0.74 \pm .06	0.47 \pm .04	0.45 \pm .05	0.84 \pm .05
Bayes-QLAE	0.60 \pm .03	0.56 \pm .03	0.71 \pm .04	0.48 \pm .03	0.47 \pm .03	0.81 \pm .03

Table 2: Disentanglement metrics measured in InfoMEC and DCI for MPI3D dataset. For each metric a higher score is better. The scores for all the models were averaged across 5 runs with different random seeds with intervals denoting 95% confidence intervals of the mean estimated assuming a t-distribution.

4 RELATED WORKS

The challenge of separating mutually independent sources in data traces back to the classical statistical problem of Independent Component Analysis (ICA) Comon (1994); Hyvärinen & Oja (2000). This core problem was later reinterpreted in the context of modern machine learning as disentanglement, formally articulated by Bengio Bengio (2013) and formalized by Higgins et al. (2018). When the data generating process is governed by nonlinear transformations Hyvärinen & Pajunen (1999), the task of learning disentangled representations becomes theoretically unidentifiable Hyvärinen & Oja (2000); Khemakhem et al. (2020); Locatello et al. (2019b). Consequently, the incorporation of auxiliary data Hyvärinen & Pajunen (1999); Hyvärinen et al. (2019); Khemakhem et al. (2020) or weak supervision Shu et al. (2019); Locatello et al. (2020) is necessary to achieve identifiability in disentanglement. A distinct line of research focuses on the incorporation of inductive biases either in the model, training objective, or the data (Locatello et al., 2019b) for identifiability.

Information-theoretic Regularization Biases. Many early and influential works leverage information-theoretic constraints on the latent space to encourage factorization. The β -VAE variants Higgins et al. (2017); Burgess et al. (2018) introduces a scalar multiplicative factor on the KL divergence penalty with isotropic Gaussian priors, forming an information bottleneck, limiting the amount of information each latent can capture. Extensions like FactorVAE Kim & Mnih (2018) and

¹The code can be found here

432 β -TCVAE Chen et al. (2018) further refine these constraints by explicitly penalizing total correlation
 433 to enforce statistical independence between dimensions. BioAE (Whittington et al., 2022) demon-
 434 strates that biologically inspired constraints, specifically, minimizing latent activity and weight en-
 435 ergy while promoting latent non-negativity encourage more factorized representations. In a similar
 436 vein, temporal sparsity is used to encourage the learning of factors varying independently across
 437 sequences (Sprekeler et al., 2014; Klindt et al., 2020).

438 **Architectural and Structural Biases.** Structural inductive biases embedded directly into model
 439 architectures have proved powerful. Vector quantization in models like QLAE (Hsu et al., 2024a)
 440 and the recent Tripod framework (Hsu et al., 2024b) induce grid-like latent spaces that simplify
 441 factor separation. FactorQLAE (Baykal et al., 2024) combine scalar quantization of the latent vari-
 442 ables with a total correlation term in the optimization as an inductive bias. On the theoretical front,
 443 Barin-Pacela et al. (2024) establish identifiability for quantized factors under nonlinear mappings.
 444 Further, Leeb et al. (2020) demonstrate that restricting different latents to enter the decoding com-
 445 putation graph at different points can enable disentanglement. Diffusion-based architectural biases
 446 have emerged as particularly effective inductive structures. Yang et al. (2023) introduce the first un-
 447 supervised framework for disentangling pre-trained diffusion models by automatically discovering
 448 latent factors and decomposing gradient fields into factor-conditioned sub-gradients. Further, Yang
 449 et al. (2024) show that diffusion models with cross-attention mechanisms serve as strong inductive
 450 biases, relying on the inherent information bottlenecks in the diffusion process and cross-attention
 451 mechanisms. Dynamic Gaussian Anchoring in Jun et al. (2025) bias towards a cluster structure in
 452 the latent space of diffusion models with cross-attention mechanisms for better separability between
 453 factor variations. Compositional constraints offer another structural approach, where maximizing
 454 the validity of composite images generated through stochastic mixing operators between latent rep-
 455 resentations enforces meaningful factor recombination without factor-specific architectural biases
 (Jung et al., 2025).

456 Recent work emphasizes the incorporation of multiple, complementary inductive biases, for exam-
 457 ple, Tripod integrates quantization, statistical independence, and inter-latent influence minimization
 458 into a single framework Hsu et al. (2024b). Similarly, our work combines complementary inductive
 459 biases derived from nonparametric priors, structured variational inference, and stochastic quanti-
 460 zation, within a principled Bayesian framework with a unified objective that provides theoretical
 461 grounding for their integration.

463 5 CONCLUSION

465 In this paper, we introduce a novel approach that incorporates Bayesian nonparametric priors into
 466 the embedding space of latent quantizing autoencoders. By leveraging the flexibility of nonpara-
 467 metric Bayesian methods, our approach enables the model to adaptively partition the latent space in
 468 accordance with the underlying data complexity, promoting more interpretable and structured latent
 469 encodings. This prior biases the learned representations toward capturing the underlying structure
 470 inherent in the data, thereby facilitating the learning of disentangled representations.

471 To enable accurate posterior inference under this flexible and hierarchical prior, we introduce a tai-
 472 lored nested and structured variational family. This variational family is specifically designed to
 473 preserve both the hierarchical structure of the prior and the inductive bias imposed by latent quan-
 474 tization, ensuring that the inference procedure remains expressive enough to capture complex depen-
 475 dencies while maintaining the structural properties essential for effective representation learning.

477 Our ablation studies systematically isolate and quantify the inductive biases contributed by each
 478 component of our hierarchical Bayesian nonparametric framework—namely, the nested variational
 479 family, structured variational inference, and stochastic quantization. Bayes-QLAE consistently out-
 480 performs all ablated variants across disentanglement metrics, demonstrating that each component
 481 provides complementary inductive biases that, when combined, enhance distinct aspects of disen-
 482 tanglement. Our empirical results demonstrate the effectiveness and generalizability of the pro-
 483 posed approach across image datasets characterized by diverse factor variation distributions. Bayes-
 484 QLAE consistently achieves superior or competitive performance relative to baseline methods on
 485 both 3DShapes and MPI3D, particularly in terms of both modularity and compactness-based disen-
 486 tanglement metrics. Importantly, this performance is attained solely through architectural inductive
 487 biases, without reliance on additional computationally expensive regularization.

486 The differential in performance on the two datasets suggests that the underlying distributional prop-
 487 erties of generative factors significantly influence the efficacy of the nonparametric prior. We hy-
 488 pothesize that replacing the Dirichlet Process prior with a more flexible prior such as the Pitman–Yor
 489 process—which allows for richer clustering structure and can model power-law behaviors—may
 490 yield further performance improvements. These findings highlight the potential of our framework
 491 for interpretable and structured representation learning in varied settings.

492
 493 REFERENCES
 494

495 Kingma DP Ba J Adam et al. A method for stochastic optimization. *arXiv preprint arXiv:1412.6980*,
 496 1412(6), 2014.

497 Charles E Antoniak. Mixtures of dirichlet processes with applications to bayesian nonparametric
 498 problems. *The annals of statistics*, pp. 1152–1174, 1974.

499
 500 Vitória Barin-Pacela, Kartik Ahuja, Simon Lacoste-Julien, and Pascal Vincent. On the identifiability
 501 of quantized factors. In *Causal Learning and Reasoning*, pp. 384–422. PMLR, 2024.

502 Gulcin Baykal, Melih Kandemir, and Gozde Unal. Disentanglement with factor quantized varia-
 503 tional autoencoders. *arXiv preprint arXiv:2409.14851*, 2024.

504
 505 Yoshua Bengio. Deep learning of representations: Looking forward. In *International conference on*
 506 *statistical language and speech processing*, pp. 1–37. Springer, 2013.

507
 508 David M Blei and Michael I Jordan. Variational inference for dirichlet process mixtures. 2006.

509
 510 Chris Burgess and Hyunjik Kim. 3d shapes dataset. <https://github.com/deepmind/3dshapes-dataset/>,
 511 2018.

512 Christopher P Burgess, Irina Higgins, Arka Pal, Loic Matthey, Nick Watters, Guillaume Des-
 513 jardins, and Alexander Lerchner. Understanding disentangling in *beta-vae*. *arXiv preprint*
 514 *arXiv:1804.03599*, 2018.

515
 516 Ruichu Cai, Zijian Li, Pengfei Wei, Jie Qiao, Kun Zhang, and Zhifeng Hao. Learning disentangled
 517 semantic representation for domain adaptation. In *IJCAI: proceedings of the conference*, volume
 2019, pp. 2060, 2019.

518
 519 Ricky TQ Chen, Xuechen Li, Roger B Grosse, and David K Duvenaud. Isolating sources of disen-
 520 tanglement in variational autoencoders. *Advances in neural information processing systems*, 31,
 521 2018.

522
 523 De Cheng, Zhipeng Xu, Xinyang Jiang, Nannan Wang, Dongsheng Li, and Xinbo Gao. Disentangled
 524 prompt representation for domain generalization. In *Proceedings of the IEEE/CVF Conference*
 525 *on Computer Vision and Pattern Recognition*, pp. 23595–23604, 2024.

526
 527 Pierre Comon. Independent component analysis, a new concept? *Signal processing*, 36(3):287–314,
 528 1994.

529
 530 Alexander D’Amour, Katherine Heller, Dan Moldovan, Ben Adlam, Babak Alipanahi, Alex Beutel,
 531 Christina Chen, Jonathan Deaton, Jacob Eisenstein, Matthew D Hoffman, et al. Underspecification
 532 presents challenges for credibility in modern machine learning. *Journal of Machine Learning*
 533 *Research*, 23(226):1–61, 2022.

534
 535 Cian Eastwood and Christopher KI Williams. A framework for the quantitative evaluation of disen-
 536 tangled representations. In *6th International Conference on Learning Representations*, 2018.

537
 538 Thomas S Ferguson. A bayesian analysis of some nonparametric problems. *The annals of statistics*,
 539 pp. 209–230, 1973.

540
 541 Muhammad Waleed Gondal, Manuel Wuthrich, Djordje Miladinovic, Francesco Locatello, Mar-
 542 tin Breidt, Valentin Volchkov, Joel Akpo, Olivier Bachem, Bernhard Schölkopf, and Stefan
 543 Bauer. On the transfer of inductive bias from simulation to the real world: a new disentan-
 544 glement dataset. In H. Wallach, H. Larochelle, A. Beygelzimer, F. d’Alché-Buc, E. Fox, and

540 R. Garnett (eds.), *Advances in Neural Information Processing Systems*, volume 32. Curran As-
 541 sociates, Inc., 2019. URL <https://proceedings.neurips.cc/paper/2019/file/d97d404b6119214e4a7018391195240a-Paper.pdf>.

542

543

544 Alex Graves. Generating sequences with recurrent neural networks. *arXiv preprint*
 545 *arXiv:1308.0850*, 2013.

546

547 Irina Higgins, Loic Matthey, Arka Pal, Christopher Burgess, Xavier Glorot, Matthew Botvinick,
 548 Shakir Mohamed, and Alexander Lerchner. beta-vae: Learning basic visual concepts with a
 549 constrained variational framework. In *International conference on learning representations*, 2017.

550

551 Irina Higgins, David Amos, David Pfau, Sebastien Racaniere, Loic Matthey, Danilo Rezende,
 552 and Alexander Lerchner. Towards a definition of disentangled representations. *arXiv preprint*
 553 *arXiv:1812.02230*, 2018.

554

555 Matthew D Hoffman and David M Blei. Structured stochastic variational inference. In *Artificial*
 556 *Intelligence and Statistics*, pp. 361–369, 2015.

557

558 Matthew D Hoffman, David M Blei, Chong Wang, and John Paisley. Stochastic variational infer-
 559 ence. *Journal of Machine Learning Research*, 2013.

560

561 Kyle Hsu, William Dorrell, James Whittington, Jiajun Wu, and Chelsea Finn. Disentanglement via
 562 latent quantization. *Advances in Neural Information Processing Systems*, 36, 2024a.

563

564 Kyle Hsu, Jubayer Ibn Hamid, Kaylee Burns, Chelsea Finn, and Jiajun Wu. Tripod: Three
 565 complementary inductive biases for disentangled representation learning. *arXiv preprint*
 566 *arXiv:2404.10282*, 2024b.

567

568 Aapo Hyvärinen and Erkki Oja. Independent component analysis: algorithms and applications.
 569 *Neural networks*, 13(4-5):411–430, 2000.

570

571 Aapo Hyvärinen and Petteri Pajunen. Nonlinear independent component analysis: Existence and
 572 uniqueness results. *Neural networks*, 12(3):429–439, 1999.

573

574 Aapo Hyvärinen, Hiroaki Sasaki, and Richard E. Turner. Nonlinear ica using auxiliary variables
 575 and generalized contrastive learning. In *Proceedings of the 22nd International Conference on*
 576 *Artificial Intelligence and Statistics (AISTATS)*, volume 89, pp. 859–868, 2019.

577

578 Matthew J Johnson, David K Duvenaud, Alex Wiltschko, Ryan P Adams, and Sandeep R Datta.
 579 Composing graphical models with neural networks for structured representations and fast infer-
 580 ence. *Advances in neural information processing systems*, 29, 2016.

581

582 Youngjun Jun, Jiwoo Park, Kyobin Choo, Tae Eun Choi, and Seong Jae Hwang. Disentangling disen-
 583 tangled representations: Towards improved latent units via diffusion models. In *2025 IEEE/CVF*
 584 *Winter Conference on Applications of Computer Vision (WACV)*, pp. 3559–3569. IEEE, 2025.

585

586 Whie Jung, Dong Hoon Lee, and Seunghoon Hong. Disentangled representation learning via mod-
 587 ular compositional bias. *arXiv preprint arXiv:2510.21402*, 2025.

588

589 Ilyes Khemakhem, Diederik Kingma, Ricardo Pio Monti, and Aapo Hyvärinen. Variational au-
 590 toencoders and nonlinear ica: A unifying framework. In *Proceedings of the 23rd Interna-*
 591 *tional Conference on Artificial Intelligence and Statistics (AISTATS)*, pp. 2207–2217, 2020. URL
 592 <https://proceedings.mlr.press/v119/khemakhem20a.html>.

593

594 Hyunjik Kim and Andriy Mnih. Disentangling by factorising. In *International conference on ma-*
 595 *chine learning*, pp. 2649–2658. PMLR, 2018.

596

597 Bohdan Kivva, Goutham Rajendran, Pradeep Ravikumar, and Bryon Aragam. Identifiability of deep
 598 generative models without auxiliary information. *Advances in Neural Information Processing*
 599 *Systems*, 35:15687–15701, 2022.

600

601 David Klindt, Lukas Schott, Yash Sharma, Ivan Ustyuzhaninov, Wieland Brendel, Matthias Bethge,
 602 and Dylan Paiton. Towards nonlinear disentanglement in natural data with temporal sparse coding.
 603 *arXiv preprint arXiv:2007.10930*, 2020.

594 Kenichi Kurihara, Max Welling, and Nikos Vlassis. Accelerated variational dirichlet process mix-
 595 tures. *Advances in neural information processing systems*, 19, 2006.
 596

597 Felix Leeb, Giulia Lanzillotta, Yashas Annadani, Michel Besserve, Stefan Bauer, and Bernhard
 598 Schölkopf. Structure by architecture: Structured representations without regularization. *arXiv*
 599 *preprint arXiv:2006.07796*, 2020.

600 Haoyang Li, Xin Wang, Zeyang Zhang, Haibo Chen, Ziwei Zhang, and Wenwu Zhu. Disentangled
 601 graph self-supervised learning for out-of-distribution generalization. In *Forty-first International*
 602 *Conference on Machine Learning*, 2024.

603

604 Francesco Locatello, Gabriele Abbati, Thomas Rainforth, Stefan Bauer, Bernhard Schölkopf, and
 605 Olivier Bachem. On the fairness of disentangled representations. *Advances in neural information*
 606 *processing systems*, 32, 2019a.

607

608 Francesco Locatello, Stefan Bauer, Mario Lucic, Gunnar Raetsch, Sylvain Gelly, Bernhard
 609 Schölkopf, and Olivier Bachem. Challenging common assumptions in the unsupervised learning
 610 of disentangled representations. In *International Conference on Machine Learning*, pp. 4114–
 611 4124, 2019b.

612

613 Francesco Locatello, Ben Poole, Gunnar Rätsch, Bernhard Schölkopf, Olivier Bachem, and Michael
 614 Tschannen. Weakly-supervised disentanglement without compromises. In *International confer-
 615 ence on machine learning*, pp. 6348–6359. PMLR, 2020.

616 Stephan Mandt, Matthew D Hoffman, and David M Blei. Stochastic gradient descent as approximate
 617 bayesian inference. *Journal of Machine Learning Research*, 18(134):1–35, 2017.

618

619 Jayaram Sethuraman. A constructive definition of dirichlet priors. *Statistica sinica*, pp. 639–650,
 620 1994.

621

622 Rui Shu, Yining Chen, Abhishek Kumar, Stefano Ermon, and Ben Poole. Weakly supervised disen-
 623 tanglement with guarantees. *arXiv preprint arXiv:1910.09772*, 2019.

624

625 Henning Sprekeler, Tiziano Zito, and Laurenz Wiskott. An extension of slow feature analysis for
 626 nonlinear blind source separation. *The Journal of Machine Learning Research*, 15(1):921–947,
 627 2014.

628

629 Vu-Hoang Tran and Ching-Chun Huang. Domain adaptation meets disentangled representation
 630 learning and style transfer. In *2019 IEEE International Conference on Systems, Man and Cyber-
 631 netics (SMC)*, pp. 2998–3005. IEEE, 2019.

632

633 Frederik Träuble, Elliot Creager, Niki Kilbertus, Francesco Locatello, Andrea Dittadi, Anirudh
 634 Goyal, Bernhard Schölkopf, and Stefan Bauer. On disentangled representations learned from
 635 correlated data. In *International conference on machine learning*, pp. 10401–10412. PMLR,
 636 2021.

637

638 Aaron Van Den Oord, Oriol Vinyals, et al. Neural discrete representation learning. *Advances in*
 639 *neural information processing systems*, 30, 2017.

640

641 Sjoerd Van Steenkiste, Francesco Locatello, Jürgen Schmidhuber, and Olivier Bachem. Are disen-
 642 tangled representations helpful for abstract visual reasoning? *Advances in neural information*
 643 *processing systems*, 32, 2019.

644

645 Martin J Wainwright, Michael I Jordan, et al. Graphical models, exponential families, and variational
 646 inference. *Foundations and Trends® in Machine Learning*, 1(1–2):1–305, 2008.

647

648 Tsun-Hsuan Wang, Wei Xiao, Tim Seyde, Ramin Hasani, and Daniela Rus. Measuring interpretabil-
 649 ity of neural policies of robots with disentangled representation. In Jie Tan, Marc Toussaint, and
 650 Kourosh Darvish (eds.), *Proceedings of The 7th Conference on Robot Learning*, volume 229 of
 651 *Proceedings of Machine Learning Research*, pp. 602–641. PMLR, 06–09 Nov 2023.

648 Yixin Wang, David Blei, and John P Cunningham. Posterior collapse and latent variable non-
 649 identifiability. In M. Ranzato, A. Beygelzimer, Y. Dauphin, P.S. Liang, and J. Wortman Vaughan
 650 (eds.), *Advances in Neural Information Processing Systems*, volume 34, pp. 5443–5455. Cur-
 651 ran Associates, Inc., 2021. URL https://proceedings.neurips.cc/paper_files/paper/2021/file/2b6921f2c64dee16ba21ebf17f3c2c92-Paper.pdf.

652
 653 James CR Whittington, Will Dorrell, Surya Ganguli, and Timothy EJ Behrens. Disentanglement
 654 with biological constraints: A theory of functional cell types. *arXiv preprint arXiv:2210.01768*,
 655 2022.
 656

657 Tao Yang, Yuwang Wang, Yan Lu, and Nanning Zheng. Disdiff: Unsupervised dis-
 658 entanglement of diffusion. In *Advances in Neural Information Processing Systems*
 659 (*NeurIPS*) 37, 2023. URL <https://proceedings.neurips.cc/paper/2023/file/da47bfaf3f3a8d5bbab0d60c5195dc18-Paper-Conference.pdf>.

660
 661 Tao Yang, Yuwang Wang, Yan Lu, and Nanning Zheng. Diffusion model with cross attention as an
 662 inductive bias for disentanglement. *NeurIPS*, 2024.
 663

664 Yuan Zhou, Richang Hong, Yanrong Guo, Lin Liu, Shijie Hao, and Hanwang Zhang. Controllable
 665 relation disentanglement for few-shot class-incremental learning. *IEEE Transactions on Circuits*
 666 and *Systems for Video Technology*, 2025.

667
 668 Xinqi Zhu, Chang Xu, and Dacheng Tao. Where and what? examining interpretable disentangled
 669 representations. In *Proceedings of the IEEE/CVF conference on computer vision and pattern*
 670 *recognition*, pp. 5861–5870, 2021.
 671

672 A APPENDIX

674 A.1 PRELIMINARIES

676 For a theoretical foundation for our proposed approach, we first review the Dirichlet Process and
 677 its role as a nonparametric prior in mixture models, with particular emphasis on the natural cluster-
 678 ing structure that emerges from this formulation. Subsequently, we discuss the quantization-based
 679 generative model, the VQ-VAE, which utilizes discrete latent representation spaces and review prior
 680 work leveraging this quantization-structure for learning disentangled representations.
 681

682 A.1.1 DIRICHLET PROCESS MIXTURE MODELS

683 We begin by considering nonparametric models, defined by an infinite-dimensional parameter space
 684 that fundamentally allows the model’s complexity to adapt and grow with the data. These models
 685 are typically used as priors over distributions with broad support that encompasses the entire space
 686 of all possible distributions. The Dirichlet Process (DP), in particular, is a stochastic process whose
 687 realizations are discrete probability distributions, thereby defining a valid nonparametric prior prob-
 688 ability distribution over the space of discrete probability measures. Sethuraman (1994) constructive
 689 definition of the DP represents each discrete distribution drawn from the DP as a weighted sum of
 690 countably infinite atomic measures sampled from a continuous base distribution. This definition
 691 uses the stick-breaking construction, where the infinite sequence of weights for the atomic measures
 692 of the discrete distribution is generated by iteratively partitioning a unit-length stick. In the first
 693 step, a segment of length β_1 is broken off the stick, where β_1 is drawn from a Beta distribution,
 694 $\beta_1 \sim \text{Beta}(1, \alpha)$, parameterized by α , ensuring $\beta_1 \in (0, 1)$. This segment is assigned as the weight
 695 of the first atomic measure θ_1 , which is independently sampled from a base distribution $G_0(\lambda)$ with
 696 parameters λ . The remaining portion of the stick, with length $1 - \beta_1$, is then recursively partitioned
 697 in the same manner: at each step, a segment of length $\beta_i \sim \text{Beta}(1, \alpha)$, scaled to the length of the re-
 698 maining stick given by $\prod_{j=1}^{i-1} (1 - \beta_j)$, is broken off and assigned as the weight of an atomic measure
 699 θ_i , drawn independently from the base distribution. This explicit stick-breaking construction gen-
 700 erates a random discrete distribution $G \sim \text{DP}(\alpha, G_0)$ over the countably infinite atomic measures
 701 θ drawn from the base distribution G_0 . Building on this, the DP serves as the nonparametric prior
 702 over the mixture components in the Dirichlet Process Mixture Models (DPMMs) Antoniak (1974).
 703 DPMMs generate data by first sampling a discrete distribution G from the prior $\text{DP}(\alpha, G_0)$ using

702 the stick-breaking construction and then using the set of atomic measures θ sampled from the base
 703 distribution G_0 to parameterize a data-generating distribution F . To generate each data point, we
 704 first sample a latent variable z from the discrete distribution defined by the stick-breaking weights,
 705 then use the corresponding atomic measure θ_z to parameterize the data-generating distribution F ,
 706 which is further used to draw the observation x :

$$707 \quad \beta_k \mid \alpha \sim p(\beta_k \mid \alpha) = \text{Beta}(1, \alpha), \quad \theta_k \mid \lambda \sim p(\theta_k \mid \lambda) = G_0(\lambda), \quad \forall k \in \mathbb{N} \quad (11)$$

$$709 \quad z = k \mid \beta \sim p(z = k \mid \beta) = \beta_k \prod_{j=1}^{k-1} (1 - \beta_j), \quad x \mid \{z, \theta\} \sim p(x \mid z, \theta) = F(\theta_z) \quad (12)$$

712 Because each realization G drawn from the DP is a discrete distribution over the atomic measures
 713 θ , the above data-generating process results in repeated parameter values for the data-generating
 714 function F . This effectively induces a partitioning of the data, where each partition or component
 715 corresponds to the data points generated with identical parameter values, allowing the generative
 716 process to be interpreted as a mixture model. Consequently, this results in a hierarchical Bayesian
 717 framework, where the parameters of the data-generating distribution F are sampled from a discrete
 718 probability distribution drawn from the DP. The joint distribution of the data $\{x_1, \dots, x_N\}$ and the
 719 latent variables: stick-breaking lengths $\beta = \{\beta_1, \beta_2, \dots\}$, component parameters $\theta = \{\theta_1, \theta_2, \dots\}$
 720 and assignment variables $\{z_1, \dots, z_N\}$, factorizes hierarchically as follows:

$$721 \quad p(x, z, \beta, \theta \mid \alpha, \lambda) = p(\beta \mid \alpha) p(\theta \mid \lambda) p(z \mid \beta) p(x \mid z, \theta) \quad (13)$$

722 The primary objective of the learning process is to infer the posterior distribution of the latent vari-
 723 ables β , θ and z conditioned on the observed data x and the hyperparameters α , λ , denoted by
 724 $p(\beta, \theta, z \mid x, \alpha, \lambda)$.

726 Computing the exact posterior over the latent variables given the observed data introduces dependen-
 727 cies among the variables. As a consequence evaluating the marginal likelihood of the data requires
 728 integrating over every possible latent configuration, making it intractable. In the nonparametric set-
 729 ting, such as under a Dirichlet Process (DP) prior, the posterior cannot be computed exactly and
 730 must be approximated. Wainwright et al. (2008) introduce a deterministic approach to approximate
 731 the intractable posterior with a simpler, tractable family of distributions by breaking certain depen-
 732 dencies among latent variables. They define a variational family q_ν , parameterized by free parameters
 733 ν , and optimize ν to minimize the Kullback–Leibler divergence between q_ν and the true posterior.
 734 Equivalently, this corresponds to maximizing the evidence lower bound (ELBO) on the log marginal
 735 likelihood of the data, as defined below:

$$735 \quad \log p(x \mid \alpha, \lambda) \geq \mathbb{E}_{q_\nu} [\log p(x, e, z, \beta, \theta \mid \alpha, \lambda) - \log q_\nu(e, z, \beta, \theta)] \quad (14)$$

737 A.1.2 VECTOR QUANTIZATION FOR DISENTANGLEMENT

739 Next, we discuss the Vector Quantized-Variational AutoEncoder (VQ-VAE) Van Den Oord et al.
 740 (2017), a generative model which learns a discrete latent representation via vector quantisation (VQ).
 741 The VQ-VAE model discretizes the continuous encoder outputs $z_e(x)$ by mapping them to a discrete
 742 latent space consisting of a codebook with a finite set of K embedding vectors $\{e_k\}_{k=1}^K$. The
 743 posterior distribution $q(z \mid x)$ of the latent variable z is categorical over the embedding space, with
 744 probabilities determined by the Euclidean distances between the encoder output and the embedding
 745 vectors in the codebook. Samples drawn from this distribution index the set of embedding vectors,
 746 which are then passed as input to the decoder z_q as follows:

$$747 \quad q(z = k \mid x) = \begin{cases} 1 & \text{for } k = \arg \min_j \|z_e(x) - e_j\|_2, \\ 0 & \text{otherwise,} \end{cases} \quad (15)$$

$$750 \quad z \sim q(z \mid x), \quad z_q(x) = e_z = e_k \quad (16)$$

751 To enable gradient propagation through the non-differentiable quantization step, a straight-through
 752 estimator is used, wherein gradients from the decoder are directly propagated back to the encoder
 753 output $z_e(x)$. The loss function used to train the VQ-VAE, defined in equation 17, consists of the re-
 754 construction loss, jointly optimizing the encoder and decoder to maximize the evidence lower bound
 755 (ELBO) on the data log-likelihood. Assuming a uniform prior $p(z)$ and a deterministic posterior as
 in equation 15, the KL divergence of the ELBO simplifies to the constant $\log K$ and is ignored. The

second term corresponds to the vector quantization loss, which updates the embedding vectors by moving them toward the encoder outputs. The third term is the commitment loss, encouraging the encoder outputs to remain close to the selected embeddings and thereby ensuring alignment between the encoder space and the embedding space.

$$L = -\log p(x | z_q(x)) + \|\text{sg}[z_e(x)] - e\|_2^2 + \beta \|z_e(x) - \text{sg}[e]\|_2^2, \quad (17)$$

where sg stands for the stop-gradient operator which blocks the gradient from propagating through the computational branch of the operand, treating it as a constant. While standard VQ-VAE approaches discretize the latent representations using a single codebook of high-dimensional embedding vector and optimize primarily for reconstruction fidelity, learning disentangled representations necessitates strong inductive biases Locatello et al. (2019b). To structure the latent space such that distinct dimensions capture independent generative factors, the approach of Hsu et al. (2024a) instead propose latent quantization, which enforces structural regularity in the latent space by quantizing each latent dimension using separate learnable scalar codebooks. Specifically, the proposed quantized latent autoencoder (QLAE) parameterizes the latent space as the Cartesian product $Z = C_1 \times \dots \times C_d$, where each codebook C_j contains scalar embeddings. This element-wise quantization enforces a combinatorial factorized encoding, allowing the decoder to learn consistent interpretations for each latent dimension. Furthermore, a higher weight decay is used to regularize the model to encourage reliance on the discrete codebook structure. Collectively, these design choices promote disentangled representations through explicit architectural and regularization biases.

A.2 ABLATION STUDIES

Model	Info M	Info C	Info E
Bayes-QLAE	$0.58 \pm .04$	$0.51 \pm .03$	$0.71 \pm .04$
T-QLAE (k=10)	$0.54 \pm .04$	$0.40 \pm .03$	$0.68 \pm .04$
T-QLAE (k=50)	$0.51 \pm .06$	$0.48 \pm .05$	$0.62 \pm .06$
MF-QLAE	$0.49 \pm .04$	$0.49 \pm .04$	$0.76 \pm .04$
DQ-QLAE	$0.52 \pm .02$	$0.43 \pm .02$	$0.71 \pm .02$

Table 3: Model performance comparison across different information metrics

We structure the experiments in this section to isolate and quantify the specific inductive biases derived from each component of our hierarchical Bayesian nonparametric framework: the nested variational family, structured variational inference, and stochastic quantization. Specifically, we perform an ablation by replacing the nested variational family with a truncated one (T-QLAE) with different truncation levels K . Similarly, to evaluate the role of the structured variational family, we substitute it with a mean-field variational family (MF-QLAE), as detailed in (Johnson et al., 2016). Finally, to isolate the effect of stochastic quantization, we replace with a deterministic nearest-neighbor quantization, with the straight-through estimator used to propagate gradients through the quantization step.

From our experiments (as detailed in Table 3) Bayes-QLAE consistently outperforms its ablated variants across all disentanglement metrics, confirming that each component contributes an inductive bias which, when combined, enhances performance. For models based on truncated variational families, we observe a negative correlation between modularity and truncation level, while a positive correlation with compactness. This aligns with the intuition that representations obtained with fewer quantized values are biased toward modularity. Notably, the truncated model with $k = 10$ surpasses QLAE in modularity due to the benefits of stochastic quantization and structured variational inference, though with a slight reduction in compactness as a consequence of stochasticity. Removing structured variational inference and defaulting to deterministic quantization degrades both modularity and compactness, with the mean-field family exhibiting a more severe decline in modularity, suggesting a bias towards representation which minimize the reconstruction cost over representations adhering to structured prior distribution. Finally, deterministic quantization exacerbates posterior collapse, leading to representations with a lower compactness metric.

We empirically demonstrate that a small codebook is not a prerequisite for disentanglement and therefore need not be constrained. Critically, across all three axes of disentanglement assess-

ment— informativeness (reconstruction fidelity), modularity (independence), and compactness (one-to-one factor-dimension correspondence)—we observe that disentanglement quality remains stable or improves as the codebook size expands adaptively in response to data complexity. These findings directly challenge the common assumption that small, fixed codebooks are necessary for learning disentangled representations.

Rather, the critical factors enabling disentanglement are two structural properties: (1) the implicit regularization effect induced by discrete latent encodings, and (2) the combinatorial composition of factor-specific codes to encode representations. During early training stages, when the codebook size is small, the encoder operates under a representational bottleneck that necessitates the construction of latent representations through combinatorial composition of the restricted set of available codes. This bottleneck implicitly regularizes the learning process, strongly biasing the encoder toward allocating disjoint, factor-specific codes to each factor-specific codebook. Consequently, the learned compositional structure mirrors the underlying generative process of the dataset, wherein the set of observations arise from the cartesian product of discrete factor instantiations. This early-stage regularization effect establishes a foundation for disentanglement by enforcing a modular, compositional encoding scheme that respects the factorial structure of the data-generating distribution.

In our approach we initialize the nonparametric prior with a single code per codebook. The nested variational family provides a principled mechanism to increase the number of codes: new codes are instantiated if and only if their inclusion yields an improvement in the variational lower bound. This criterion ensures that capacity expansion occurs only when statistically justified by the data. Consequently, the model inherits the inductive bias of sparse codebooks while avoiding any explicit hard constraint on the upper bound of the cardinality of the codebooks. This adaptive regularization mechanism resolves the tension between early-stage structural learning and asymptotic expressiveness.

We validate this hypothesis through ablation studies comparing our nested variational inference framework against a truncated variant. In the truncated approach, we fix the number of mixture components at a predetermined upper bound for each factor, effectively eliminating the adaptive capacity of the nonparametric formulation. This modification results in measurable degradation across all disentanglement metrics relative to the nested variational inference approach. These results demonstrate that the adaptive, data-driven discovery of codebook size—rather than absolute codebook cardinality—is the essential mechanism underlying successful disentanglement.

Moreover, the tendency toward cluster expansion is explicitly governed by the concentration parameter α of the nonparametric prior, which is itself assigned a Gamma hyperprior. This hierarchical Bayesian formulation provides regularization of the cluster proliferation rate, enabling the model to infer from data the appropriate balance between model parsimony and representational capacity without manual specification.

A.3 DISENTANGLEMENT METRICS

For quantitative evaluation, we compute two complementary disentanglement metrics which comprehensively measure disentanglement properties using different computational approaches. The InfoMEC metric (Hsu et al., 2024a) relies on information-theoretic mutual information estimation computed from the empirical joint distribution between latent representations and ground-truth factors. In contrast, the DCI metric (Eastwood & Williams, 2018) trains predictive models to map the learned representations to the underlying factors of variation. Both metrics evaluate disentanglement quality across three fundamental dimensions, though with different terminology: InfoMEC measures InfoModularity (InfoM) while DCI measures Disentanglement (D) to quantify the extent to which sources are encoded in mutually disjoint subsets of representations, InfoExplicitness (InfoE) and Informativeness (I) measure the degree to which the relationship between the sources and representations can be characterized by a simple functional or statistical dependency, and InfoCompactness (InfoC) and Completeness (C) quantifies the degree to which latent variables encode information exclusively about mutually disjoint subsets of the sources. We train our proposed approach in a completely unsupervised manner on the entire dataset and evaluate the learned representations on a subset of samples, using the open-source implementations of disentanglement metrics by Locatello et al. (2019b); Hsu et al. (2024a).

864
865

A.4 QUALITATIVE EVALUATION

866
867
868
869
870
871
872
873
874
875

We conduct qualitative assessments of our proposed method on each dataset to evaluate both sample reconstructions and latent traversals. For latent traversals, we encode a single image into the latent space and systematically visualize the effects of intervening on individual latent dimensions. Specifically, for each latent variable we vary its value across the range of values encoded in the representations (sample with replacement) while holding all other latent dimensions fixed, then decode the resulting latent vectors to observe their effects in the data space. In the visualization, each row corresponds to interventions on a single latent variable, while columns represent different values sampled from the empirical distribution of that dimension. Well-disentangled representations should exhibit smooth, semantically meaningful changes along individual latent dimensions, with each dimension controlling a distinct generative factor independently of others.

876
877
878
879
880

Reconstruction Fidelity. We assess the informativeness of learned representations by examining reconstruction quality. High-fidelity reconstructions that faithfully preserve visual details of the original images indicate that the latent representations are sufficiently informative to capture the full range of variations present in the data. Conversely, poor reconstructions suggest that certain factors of variation have been inadequately encoded or lost during the encoding process.

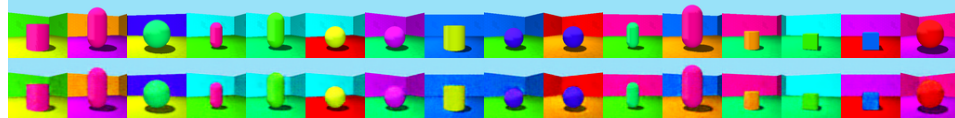
881
882
883
884
885
886
887

Modularity. We evaluate the modularity, or disentanglement, properties of learned representations through latent traversal analysis. A representation exhibits modularity when each latent dimension independently controls a single underlying generative factor while remaining invariant to variations in other factors. Operationally, this is assessed by examining whether each row in the traversal visualization demonstrates isolated semantic changes corresponding to a single factor of variation without coupling to other factors. Such independence in the latent space reflects successful recovery of the true compositional structure of the underlying independent generative factors.

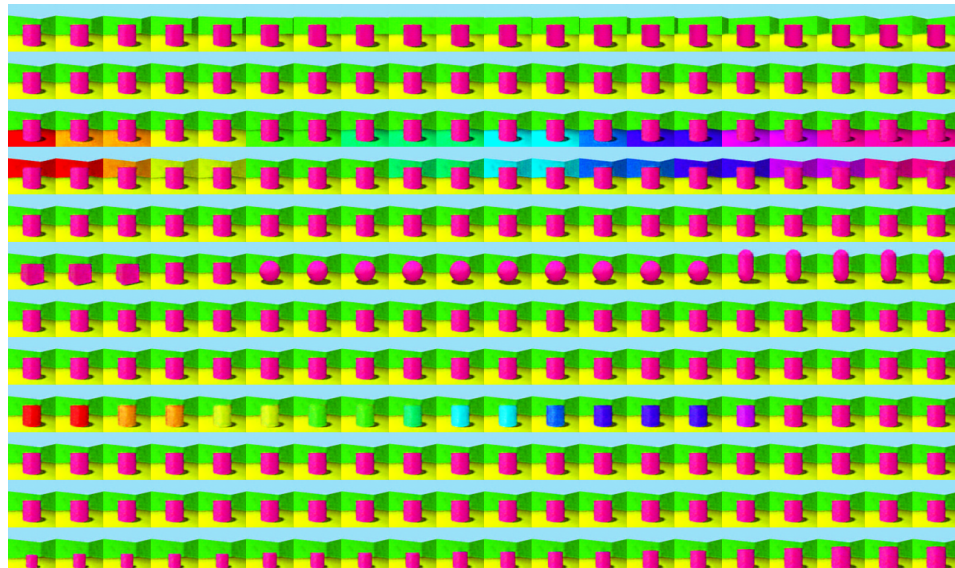
888
889
890
891
892
893
894
895
896
897
898
899
900
901
902
903
904
905
906
907
908
909
910
911
912
913
914
915
916
917

Compactness. We further assess the compactness, or completeness, of the learned representations by determining whether all variations of a single generative factor are captured within a single latent dimension. Compact representations, wherein each factor is encoded by exactly one latent variable, are crucial for interpretability as they establish a one-to-one correspondence between latent dimensions and semantically meaningful generative factors. This property enables intuitive understanding and manipulation of specific attributes in the generated outputs.

918
919
920
921
922
923
924
925
926
927



928
929
930
931
932 (a) Sample reconstructions: Original images (top row) and corresponding reconstructions (bottom row)
933



934
935
936
937
938
939
940
941
942
943
944
945
946
947
948
949
950
951
952 (b) Latent traversals: Each row shows the effect of systematically varying a single latent dimension while
953 holding all other dimensions fixed. Columns represent different values sampled from the distribution of that
954 dimension. The model successfully disentangles six ground-truth factors of variation: object orientation (row
955 1), floor hue (row 3), wall hue (row 4), object shape (row 6), object hue (row 9), and object scale (row 12).
956 Rows 2, 5, 7, 8, 10, and 11 correspond to inactive latent dimensions that do not encode interpretable factors.
957

958 Figure 1: Reconstructions and Latent traversals for the 3DShapes dataset: Reconstructions demon-
959 strate high fidelity in capturing visual details demonstrating the model’s ability to faithfully encode
960 and decode the full range of variations in the data. Latent traversals illustrate that individual latent
961 variables control distinct, interpretable factors of variation in the generated images. Moreover, the
962 presence of inactive latent variables and the encoding of each factor in a single latent variables indi-
963 cates that the model has learned a compact representation recovering the true generative structure
964
965
966
967
968
969
970
971

972

973

974

975

976

977

978

979

980

981

982

983

984

985

986

987

988

989

990

991

992

993

994

995

996

997

998

999

1000

1001

1002

1003

1004

1005

1006

1007

1008

1009

1010

1011

1012

1013

1014

1015

1016

1017

1018

1019

1020

1021

1022

1023

1024

1025

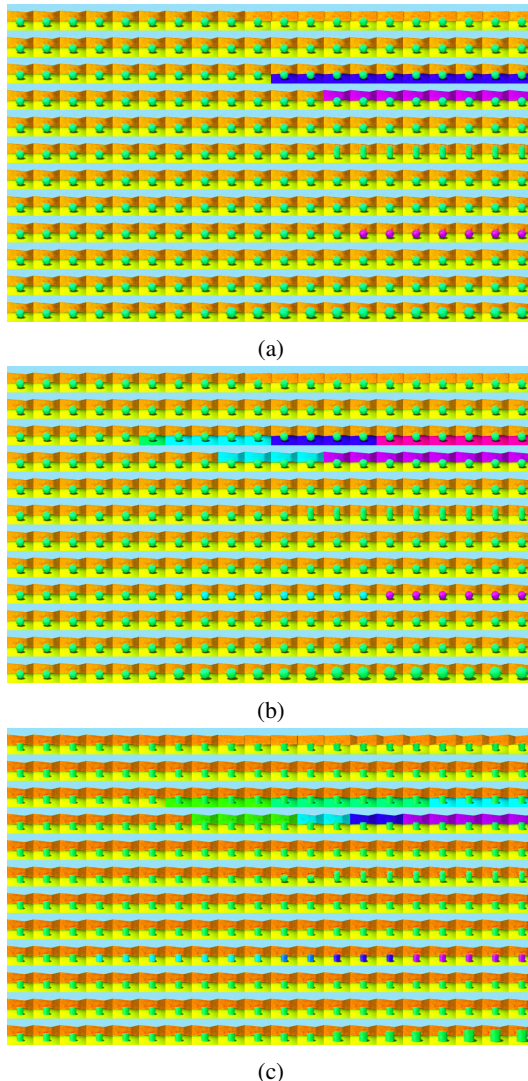
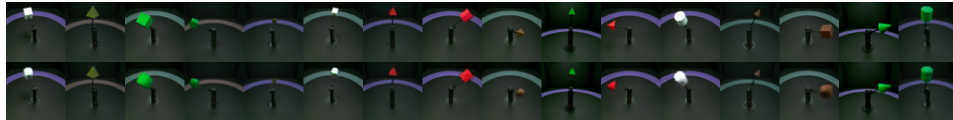


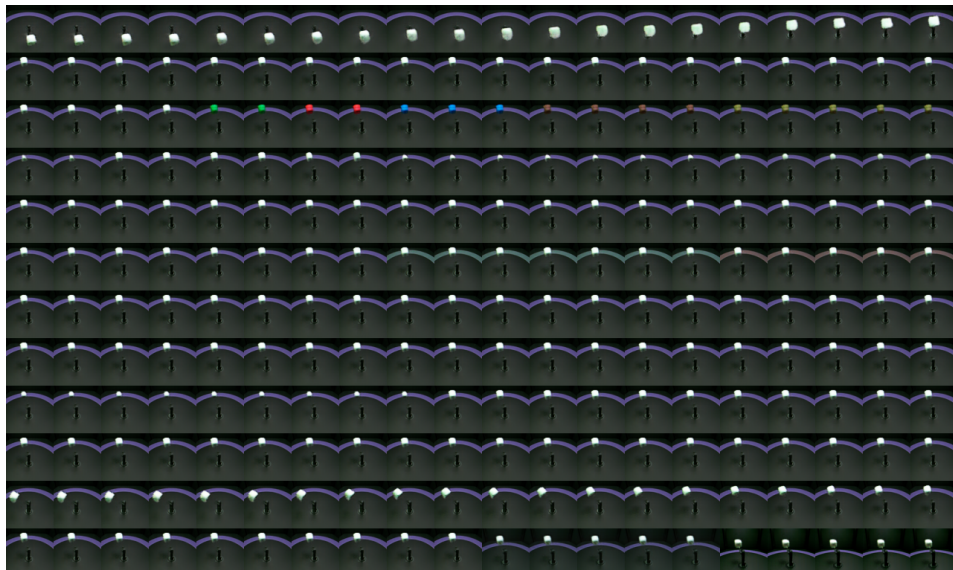
Figure 2: Evolution of Latent Traversals for 3DShapes dataset: The figure illustrates the evolution of the number of clusters associated with each generative factor demonstrating the adaptive capacity of the nonparametric formulation. Each column in each row corresponds to a factor-specific mixture component, and the distinct components within a row denote the clusters capturing the encoded variations of that factor. The vertical axis indicates cluster multiplicity, revealing how the model progressively discovers and encodes additional variations for each factor. This dynamic cluster growth exemplifies the nonparametric property of the hierarchical mixture prior, which enables data-driven inference of latent capacity without manual specification. Notably, factors with higher contribution to the reconstruction objective—such as floor hue, object hue, and wall hue—exhibit earlier cluster proliferation during training, suggesting the model prioritizes encoding variations that most significantly impact reconstruction fidelity. In contrast, geometric factors such as object orientation and shape undergo refinement in later training stages, indicating a hierarchical learning strategy wherein the model first captures high-variance attributes before refining lower-variance structural properties. This demonstrates that the nonparametric prior successfully balances model capacity across factors according to their respective complexities and contributions to data likelihood

1026
1027
1028
1029
1030
1031
1032
1033
1034
1035
1036
1037
1038



1039 (a) Sample reconstructions: Original images (top row) and corresponding reconstructions (bottom row)
1040

1041
1042
1043
1044
1045
1046
1047
1048
1049
1050
1051
1052
1053
1054
1055
1056
1057
1058



1059 (b) Latent traversals: Each row shows the effect of systematically varying a single latent dimension while
1060 holding all other dimensions fixed. Columns represent different values sampled from the distribution of that
1061 dimension. The model successfully disentangles the following ground-truth factors of variation: vertical axis
1062 (row 1), object color (row 3), object shape (row 4), background color (row 6), object size (row 9), horizontal
1063 axis (row 11) and camera height (row 12). Rows 2, 5, 7, 8, 10 correspond to inactive latent dimensions that do
1064 not encode interpretable factors.
1065

Figure 3: Reconstructions and Latent traversals for the MPI3D real dataset: Reconstructions demonstrate high fidelity in capturing visual details demonstrating the model’s ability to faithfully encode and decode the an extensive range of variations in the data. Latent traversals illustrate that individual latent variables control distinct, interpretable factors of variation in the generated images. It is worth noting that, although the representations do not capture the full set of underlying variations, they remain both modular and compact, closely reflecting the true underlying structure of the generative process.

1072
1073
1074
1075
1076
1077
1078
1079